ISSN 2411-3336; e-ISSN 2541-9404

JOURNAL OF MINING INSTITUTE

Zapiski Gornogo instituta

Journal homepage: pmi.spmi.ru

Research article

Association of quartz, Cr-pyrope and Cr-diopside in mantle xenolith in V.Grib kimberlite pipe (northern East European Platform): genetic models

Elena V. Agasheva✉, Denis S. Mikhailenko, Andrei V. Korsakov
V.S.Sobolev Institute of Geology and Mineralogy, Novosibirsk, Russia

***How to cite this article*:** Agasheva E.V., Mikhailenko D.S., Korsakov A.V. Association of quartz, Cr-pyrope and Cr-diopside in mantle xenolith in V.Grib kimberlite pipe (northern East European Platform): genetic models. Journal of Mining Institute. 2024. Vol. 268, p. 503-519.

Abstract. The first results of mineralogical and geochemical studies of a unique xenolith of lithospheric mantle are presented illustrating the earlier non-described mineral association of quartz, Cr-pyrope and Cr-diopside. Structural and textural features of the sample suggest a joint formation of these minerals. The calculated *P-T*-parameters of the formation of Cr-diopside indicate the capture of xenolith from the depth interval ~ 95-105 km (31-35 kbar) corresponding to the stability field of coesite. This suggests that quartz in the studied xenolith can represent paramorphs after coesite. It was shown that quartz in this rock is not a product of postmagmatic processes. The transformation stage of the source lherzolite into garnet- and clinopyroxene-enriched rock/garnet pyroxenite as a result of exposure to a high-temperature silicate melt was reconstructed. Subsequent stages of the influence of metasomatic agents were identified by the presence of a negative Eu-anomaly in some garnet grains, which could result from the impact of subduction-related fluid and the enrichment of rock-forming minerals with light rare earth elements, Sr, Th, U, Nb and Ta as a consequence of fluid saturated with these incompatible elements. Several models for the formation of SiO_2 phase (quartz/coesite) in association with high-chromium mantle minerals are considered including carbonatization of mantle peridotites/eclogites and melting of carbonate-containing eclogites at the stage of subduction and the impact of SiO_2-enriched melt/fluid of subduction genesis with peridotites of the lithospheric mantle.

***Keywords*:** quartz; Cr-diopside; Cr-pyrope; lithospheric mantle; mantle xenolith; mantle metasomatism; subduction; kimberlite; garnet pyroxenite; craton

Funding. Concentrations of the main and rare elements in garnet and clinopyroxene were determined with support of the Russian Science Foundation grant N 20-77-10018. Electron scanning microscopy and Raman spectroscopy were performed due to support of the Russian Science Foundation grant N 21-77-10006. Xenolith sample was taken during the field work under the state assignment at IGM SB RAS (N 122041400157-9).

Received: 04.04.2023 ***Accepted: 20.09.2023*** ***Online: 19.12.2023*** ***Published: 26.08.2024***

Introduction. Quartz is one of the most common minerals in the earth's crust and, as a rock-forming mineral occurs in a wide variety of magmatic, metamorphic, hydrothermal, hypergene and sedimentary rocks. It forms and occurs in a wide range of *P-T*-conditions [1], but its occurrence in rocks of the continental lithospheric mantle represented predominantly by high-magnesium peridotites (olivine makes up 40-100 vol.%) is very limited in the first place due to the impossible chemical equilibrium of the mineral pair olivine-SiO_2, the reaction of which results in formation of enstatite [2].

Quartz was identified as inclusions in ortho- and clinopyroxenes in a websterite xenolith from the alkali-basaltic tuff of the Bakoni-Balaton-Highland volcanic field in western Hungary [3] and as inclusions in orthopyroxene in a peridotite xenolith from alkali basalts of the Tallante Province in southern Spain [4]. Quartz in these rocks formed due to interaction of SiO_2-enriched melt of subduction genesis with peridotites of lithospheric mantle [3, 4].

Among rocks of the cratonic lithospheric mantle, SiO_2-rich varieties are coesite-bearing eclogites occurring as xenoliths in kimberlites [5]. In mantle eclogites, quartz was identified as exsolution in garnet, as inclusions in garnet and omphacite and in intergranular space as well as in garnet-quartz symplectites and was interpreted as paramorphs after coesite [6-8]. The association of olivine (Fo_{80-83}) and quartz (as a paramorph after coesite) was discovered in diamond-bearing coesite eclogite [8], and olivine in this sample formed under the influence of alkali-enriched melt related to kimberlite. The inclusion of α-quartz with olivine ($Fo_{93.5}$) and albite was discovered in diamond from Shengli N 1 kimberlite (China), and coexistence of the minerals of crustal and mantle origin in the diamond can be accounted for by the participation of a crustal subducted component during the growth of diamond [9]. An association of quartz (as a paramorph after coesite) and Cr-pyrope of the harzburgite association was discovered in one diamond crystal from the Mwadui kimberlite pipe, Tanzania [10]. The formation of mineral inclusions of mixed peridotite-eclogite paragenesis is associated with staged growth of diamond as a result of a marked change in the composition of the crystallization medium including carbonatization of peridotites [10]. Experimental works [11] show that the release of a significant amount of free SiO_2 and subsequent formation of coesite can occur at 6.5 GPa during CO_2 reaction with garnet, Na_2CO_3 and orthopyroxene at T < 1,450 °C or with orthopyroxene at T > 1,450 °C. These examples demonstrate that the occurrence of SiO_2 in the form of coesite or quartz in rocks of lithospheric mantle is associated with various factors that can indicate both the interaction of crustal and mantle matter [3, 4, 9], and the transformation of the source peridotites by metasomatic agents with formation of the mineral association of a mixed peridotite-eclogite type [8, 10].

This paper presents the first results of the mineralogical and geochemical study of a unique sample of mantle xenolith from V.Grib kimberlite pipe, which presents a previously undescribed mineral association of quartz – Cr-pyrope – Cr-diopside. Interpretation of concentrations of the main and rare elements in rock-forming minerals in xenolith is used to reconstruct the stages of rock formation and transformation [12-14] and allows proposing several models for the formation of quartz in association with high-chromium mantle minerals.

Methods. Mineralogical and petrographic study of the xenolith was accomplished in a flat-polished plate using Zeiss Axiolab-5 optical microscope equipped with a high-resolution digital camera Axiocam 208 Color, and the scanning electron microscope Tescan MIRA 3 LMU (SEM) (Tescan) equipped with an INCA microanalysis system Energy 450 XMax-80 (Oxford Instruments Ltd.) at the Analytical Center for multi-elemental and isotope research SB RAS (Novosibirsk). Raman spectra for fifteen quartz grains were obtained in the range from 50 to 4,000 cm^{-1} on the LabRam spectrometer Horiba Jobin Yvon (V.S.Sobolev Institute of Geology and Mineralogy, Novosibirsk) equipped with a laser with a wavelength of 532 nm (~10 mV) and a beam diameter of ~2 μm.

Concentrations of the main elements in garnets and clinopyroxenes were determined on JEOL JXA-8100 electron probe microanalyzer at the Analytical Center for multi-elemental and isotope research SB RAS (Novosibirsk) at an accelerating voltage 20 kV and current 50 nA with beam size 1 μm. For calibration, own natural mineral standards of V.S.Sobolev Institute of Geology and Mineralogy were used. Relative standard deviations were within 1.5 %. Data were obtained for 10 s at the peak as well as 10 s on both sides of the background; ZAF correction was applied. Detection limits were <0.05 wt.% for all the analysed elements including 0.01 wt.% for Cr and Mn, 0.02 wt.% for Ti and Na, and 0.05 wt.% for K.

Determination of rare element concentrations in garnets and clinopyroxenes was accomplished in a flat-polished section using XSERIES2 quadrupole inductively coupled plasma mass spectrometer (Thermo Scientific) combined with a 213 nm laser sampling device (New Wave Research, Nd:YAG solid-state laser) at the Analytical Centre of Novosibirsk State University. Before each determination, the analysed area of the mineral was checked in transmitted and reflected light for the absence of

cracks, microinclusions and secondary alterations. The analysis was carried out at a frequency of 20 Hz with pulse energy 12 mJ/cm^{-2} and beam size 50 μm. Helium was used as a carrier gas. Data acquisition time was 90 s per point including 30 s for background and 60 s for signal. Reference samples NIST 612 and NIST 614 were used as external standards. Instrument sensitivity drift was monitored by shooting NIST 610 as an unknown sample. Two NIST 612 standard analyses were performed before and after every ten measurements. Detection limits were higher for elements with lighter mass (Sc-Sr) ranging from 0.1 to 0.2 ppm and were 0.01 ppm for elements heavier than Sr. Ca concentrations determined by electron probe analysis were used as internal standards.

High-diamond-bearing V.Grib kimberlite pipe (376 ± 3 Ma [15]) occurs in the northern East European Platform, in the central part of the Arkhangelsk diamondiferous province (ADP), in which ~ 100 igneous bodies of mafic and ultramafic compositions were discovered. The results of comprehensive studies of igneous rocks of the ADP are presented in articles [16, 17].

Results. Sample G2-35 is an irregularly shaped 4×3×2 cm xenolith discovered in a kimberlite sample from the diatreme part of V.Grib pipe at the depth of 400 m from the surface. Xenolith G2-35 is represented by the predominant clinopyroxene of emerald-green colour (42 vol.%) and, in a smaller amount, by garnet of rich violet colour (17 vol.%). Clinopyroxene and garnet grains have irregular shapes, vary in size from 0.5 to 7 mm and are unevenly distributed in the rock (Fig.1, *a*). All garnet and clinopyroxene grains are penetrated by numerous cracks filled with a chlorite-serpentine aggregate (Fig.1, *b-e*). At the rims of some garnet grains, phlogopite occurs which also develops along garnet cracks and can partially replace it (Fig.1, g). Inside the cracks of some garnet grains, chromite grains are diagnosed having an oval-elongated shape with a size no more than 0.1 mm (Fig.1, *f*). In addition to garnet and clinopyroxene, numerous areas of light grey colour (41 vol.%) are visually identified in the rock represented by quartz grains accompanied by the development of a chlorite-serpentine aggregate (Fig.1, *a-e*; Fig.2). Quartz grains are characterized by an oval and elongated shape, their size ranging from 0.5 to 2.5 mm (Fig.1, *b-e*). Quartz grains are also found inside large grains of garnets and clinopyroxenes (Fig.1, *b-d, g*).

Garnet (Table 1) is represented by pyrope ($Alm_{13-14}Pyr_{71-76}Gross_{12-15}$) with medium-high concentrations of Cr_2O_3 (3.5-6.5 wt.%) and magnesium values Mg# = Mg/(Mg + Fe) 0.84-0.86, which allows classifying it as chromium-containing pyrope of mantle genesis [18]. By the content of CaO and Cr_2O_3, garnets correspond to the lherzolite association (Fig.3, *a* [19]). Garnets have a heterogeneous composition with varying concentrations of Cr_2O_3 (3.5-6.5 wt.%), CaO (4.4-5.9 wt.%) and Al_2O_3 (18.4-21.1 wt.%). Most grains are zoned: the central parts are characterized by higher concentrations of Cr_2O_3 and CaO and lower contents of Al_2O_3 compared to the rim parts (Fig.3, *b*). TiO_2 content does not exceed 0.05-0.15 wt.%, and Ni is in the range of 16-29 ppm (single analysis at 64 ppm), and only in one zoned grain the rim part has higher Ni concentrations (18 and 34 ppm in the centre and rim, respectively). As to the contents of rare (R) and rare earth (RE) elements (E), garnets (Table 2) show heterogeneity that does not correlate with concentrations of the main elements.

Not all garnets zoned by the main elements show different RE concentrations in the central and rim zones of grains (Fig.4, *a, b*). Three types of RE and REE distribution spectra normalized to Cl chondrite were identified in these grains [20]: with the fractionated spectrum from light (L) to heavy (H) REE (La_n/Yb_n = 0.05) with LREE concentrations at the level of 1-2 chondritic units (ch.u.); with the fractionated spectrum from LREE to HREE (La_n/Yb_n = 0.2-0.3), enrichment in the LREE region at the level of 4-6 ch.u. and negative (0.7-0.9) Eu-anomaly ($Eu_n/(Sm_n + Gd_n)/2n$); with a fractionated spectrum from medium (M) to HREE (Sm_n/Yb_n = 0.4-0.5) and enrichment in the region of LREE at the level of 7-11 ch.u. (La_n/Yb_n = 0.3-0.5). Despite the differences in the distribution pattern of RE and REE, all these grains contain identical HREE concentrations at the level of 9-25 ch.u. at values of Gd_n/Yb_n ~ 0.5 and are depleted in Sr and Ti (Fig.4, *a, b*). Grains of garnets zoned by the main and rare elements are represented by two types. The central parts of zoned garnets of the first type are characterized by lower concentrations of LREE (0.5-2 ch.u.; La_n/Yb_n = 0.02-0.08)

and Sr (0.1-0.5 ch.u.) and a negative Eu-anomaly (0.7) compared to the rim parts, which are characterized by higher LREE contents (4-8 ch.u; La_n/Yb_n = 0.2-0.4) and Sr (2-3 ch.u) and a decrease in the Eu-anomaly values (0.9; Fig.4, *c*, *d*). The central parts of zoned garnets of the second type have a fractionated spectrum from LREE to HREE (La_n/Yb_n = 0.02) with LREE content at the level of 0.5-2 ch.u. and depletion in Sr (0.05-0.1 ch.u.); the rim parts are enriched with LREE (3-4 ch.u.; La_n/Yb_n = 0.1-0.2) and Sr (1 ch.u.; Fig.4, *e*, *f*). As for HREE concentrations, all zoned garnets are identical to garnets in which RE zoning was not detected. Absolutely all garnet grains from sample G2-35 have identical concentrations of Y (22-28 ppm) and Zr (15-26 ppm) and similar values of the Zr/Hf (40-93) and Ti/Eu (780-1400) ratios. In the Y/Zr distribution (Fig.5, *a*), the composition points of garnets lie near the trend of high-temperature silicate mantle metasomatism [21].

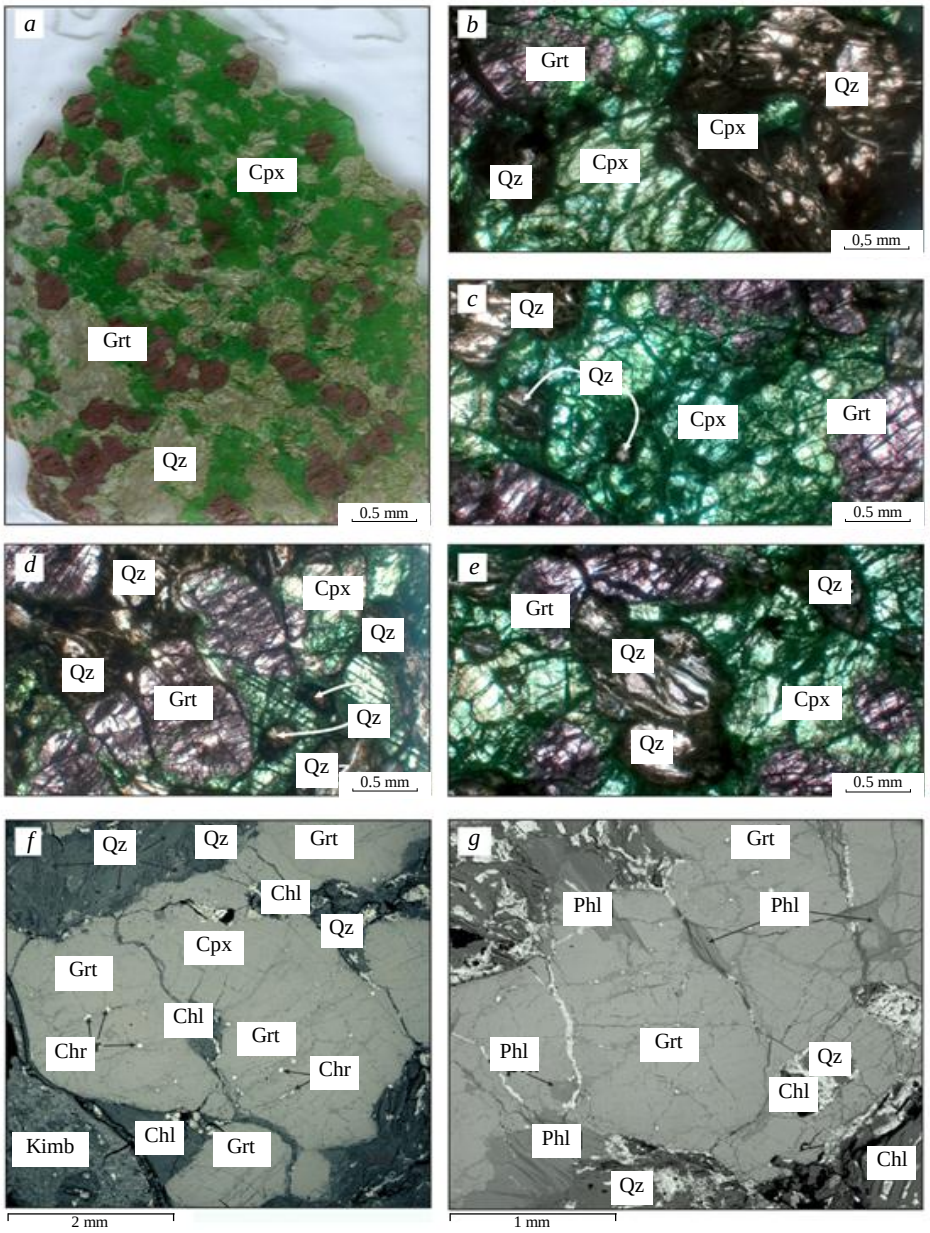

Fig.1. Mineralogical and petrographic features of xenolith G2-35:
a – general view of a flat-polished section;
b-e – images in transmitted light;
f, *g* – images in backscattered electrons
Grt – garnet; Cpx – clinopyroxene; Qz – quartz; Phl – phlogopite;
Chr – chromite; Chl – chlorite; Kimb – kimberlite

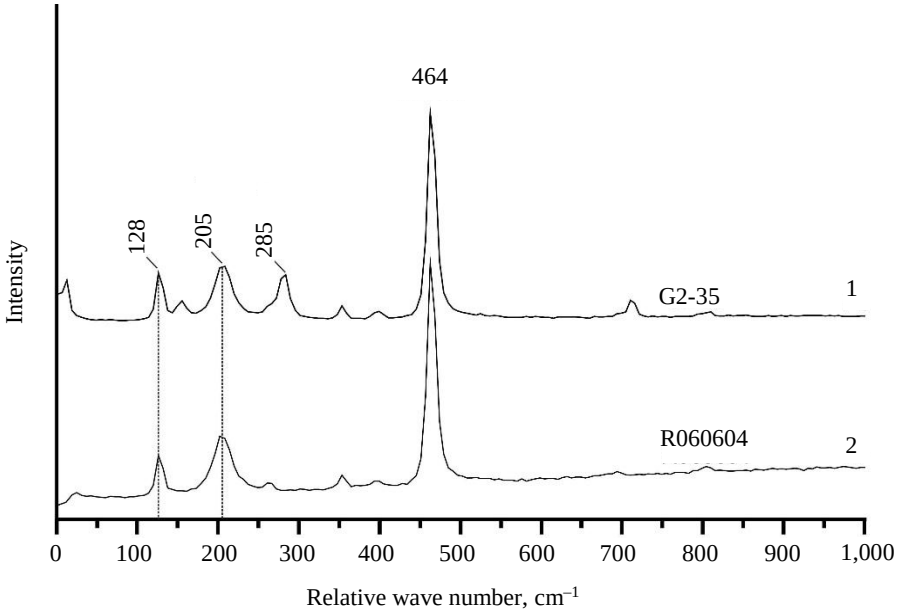

Fig.2. Representative Raman spectrum of quartz from sample G2-35 (1) and reference spectrum of quartz (2) from the international database of Raman spectra of minerals RRUFF*

Table 1

Concentration of main elements in garnets from xenolith G2-35, wt.%

Element	1 *c*	1 *r*	2 *c*	2 *r*	3 *c*	3 *r*	4 *c*	4 *r*
SiO_2	42.00	42.14	42.26	42.09	42.32	42.41	42.43	42.48
TiO_2	0.13	0.11	0.14	0.11	0.08	0.09	0.05	0.09
Al_2O_3	19.41	20.80	18.69	19.77	19.80	20.29	20.21	20.75
Cr_2O_3	5.52	4.09	6.29	5.16	4.86	4.27	4.18	3.56
FeO	6.61	6.61	6.79	6.67	6.36	6.38	6.40	6.36
MnO	0.44	0.44	0.41	0.41	0.40	0.42	0.39	0.42
MgO	20.07	20.77	19.37	20.26	20.28	20.37	20.90	20.87
CaO	5.39	4.78	5.85	5.23	5.28	4.98	4.94	4.69
Na_2O	0.05	0.08	0.07	0.09	0.10	0.00	0.03	0.00
K_2O	0.01	0.01	0.00	0.01	0.00	0.00	0.01	0.00
Total	99.63	99.83	99.87	99.79	99.47	99.21	99.55	99.23
Mg#	0.84	0.85	0.84	0.84	0.85	0.85	0.85	0.85
Element	5 *c*	5 *r*	6 *c*	7 *c*	8 *c*	9 *c*	10 *c*	11 *c*
SiO_2	41.71	42.10	42.52	42.32	42.78	42.64	42.80	42.58
TiO_2	0.14	0.10	0.06	0.09	0.05	0.05	0.05	0.09
Al_2O_3	18.39	19.57	20.30	20.49	21.04	20.91	20.49	20.63
Cr_2O_3	6.56	5.10	4.11	3.84	3.44	3.52	4.11	3.88
FeO	6.76	6.65	6.42	6.39	6.34	6.40	6.25	6.37
MnO	0.44	0.45	0.43	0.43	0.45	0.44	0.45	0.41
MgO	19.37	20.27	20.79	20.94	21.22	20.97	20.82	20.73
CaO	5.90	5.17	4.93	4.93	4.44	4.66	4.99	4.90
Na_2O	0.07	0.05	0.02	0.03	0.06	0.06	0.06	0.02
K_2O	0.01	0.00	0.01	0.00	0.01	0.00	0.00	0.00
Total	99.34	99.48	99.59	99.47	99.82	99.64	100.00	99.62
Mg#	0.84	0.84	0.85	0.85	0.86	0.85	0.86	0.85

Note: c – centre, *r* – rim of grain, 1-11 – grain number.

*RRUFF Project website. URL: https://rruff.info (accessed 21.09.2023).

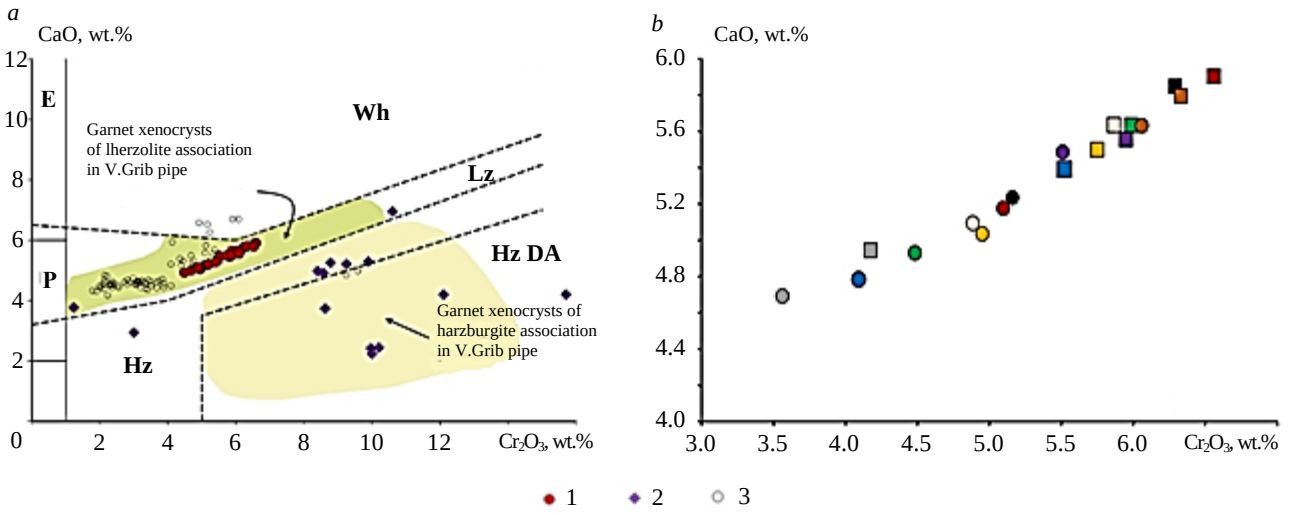

Fig.3. Concentrations of CaO and Cr_2O_3 (wt.%) in garnets from xenolith G2-35:
a – position of composition points on the diagram [19] in comparison with garnets from xenoliths of peridotites and kimberlite [22] in V.Grib pipe and inclusions in ADP diamonds; *b* – content of CaO and Cr_2O_3 in the central (square) and rim (circle) parts of nine individual garnet grains zoned in composition (the same element colour corresponds to a single grain)

1 – garnets from xenolith G2-35; 2 – garnets from inclusions in diamonds of ADP kimberlites; 3 – garnets from peridotites in V.Grib pipe; parageneses: Lz – lherzolite; Hz – harzburgite; Hz DA – harzburgite diamondiferous; Wh – wehrlite; E – eclogite; P – pyroxenite

Table 2

Concentration of rare elements in garnets and clinopyroxene from xenolith G2-35, ppm

Element	Garnet													
	1 *c*	1 *r*	2 *c*	2 *r*	3 *c*	3 *r*	4 *c*	4 *r*	5 *c*	5 *r*	6 *c*	7 *c*	8 *c*	9 *c*
Ti	667	701	552	590	677	662	616	521	608	614	587	572	604	603
Ni	19.6	22.4	22.1	16.1	18.3	34.0	18.0	17.3	22.5	28.0	20.9	22.6	64.0	28.5
Sr	0.61	16.5	3.27	20.3	0.49	7.40	0.37	7.23	4.17	12.6	6.72	24.3	23.2	35.2
Y	27.4	27.9	22.4	24.9	26.0	25.1	24.6	23.5	22.8	26.9	23.1	26.1	23.3	24.8
Zr	25.4	15.5	14.8	14.6	19.9	16.4	20.9	17.8	23.2	17.7	13.0	21.4	26.2	19.1
Nb	0.13	1.25	0.28	0.66	0.16	0.63	0.08	0.68	0.28	0.77	0.77	1.78	0.68	1.96
La	0.11	1.89	0.39	1.24	0.10	0.69	0.11	0.83	0.27	1.06	1.17	1.76	0.94	2.69
Ce	1.10	3.52	1.05	2.47	1.22	2.10	0.91	1.88	1.29	2.43	2.29	4.53	2.42	5.17
Pr	0.41	0.58	0.27	0.43	0.38	0.41	0.30	0.41	0.35	0.52	0.39	0.88	0.45	0.66
Nd	3.71	3.20	2.14	2.32	3.43	3.06	2.55	2.76	2.67	3.27	2.71	4.97	3.25	4.05
Sm	1.98	1.40	1.03	1.15	1.49	1.33	1.56	1.38	1.45	1.64	1.48	1.84	1.71	1.41
Eu	0.52	0.54	0.37	0.49	0.65	0.56	0.54	0.53	0.66	0.53	0.42	0.73	0.54	0.68
Gd	2.72	2.45	2.20	2.27	2.71	2.36	2.01	1.96	2.27	2.22	2.07	2.34	2.01	2.23
Tb	0.52	0.55	0.43	0.44	0.50	0.56	0.46	0.42	0.46	0.51	0.41	0.54	0.43	0.48
Dy	3.85	4.41	3.60	4.09	4.45	4.22	3.88	3.28	3.35	3.81	3.71	4.33	3.79	3.97
Ho	1.11	1.00	0.96	0.94	1.05	1.02	0.98	0.98	0.95	1.03	0.84	1.11	0.84	0.97
Er	3.62	3.41	2.83	3.44	3.48	3.25	3.32	3.06	3.16	3.36	2.80	3.38	3.26	3.02
Tm	0.52	0.52	0.46	0.50	0.49	0.51	0.50	0.45	0.45	0.50	0.49	0.52	0.50	0.53
Yb	3.64	3.71	3.35	3.67	3.79	3.78	3.82	3.47	3.47	3.51	3.23	3.99	3.56	3.82
Lu	0.56	0.56	0.54	0.59	0.55	0.51	0.56	0.53	0.56	0.64	0.50	0.54	0.60	0.57
Hf	0.39	0.37	0.24	0.25	0.30	0.28	0.30	0.29	0.25	0.27	0.18	0.33	0.35	0.31
Ta	0.01	0.03	0.01	0.03	0.01	0.01	0.01	0.02	0.01	0.03	0.03	0.10	0.02	0.07
Th	0.02	0.17	0.04	0.13	0.04	0.09	0.03	0.07	0.02	0.09	0.11	0.27	0.11	0.27
U	0,07	0.10	0.05	0.09	0.08	0.08	0.06	0.09	0.06	0.10	0.07	0.15	0.07	0.10

End of Table 2

Element	Clinopyroxene								
	1 *c*	2 *c*	3 *c*	4 *c*	5 *c*	6 *c*	7 *c*	8 *c*	9 *c*
Ti	694	631	682	798	690	1053	664	638	869
Ni	204	195	181	189	165	264	219	168	255
Sr	366	393	501	358	466	632	365	405	628
Y	4.62	5.19	4.52	5.14	3.73	2.34	5.21	5.58	2.76
Zr	39.0	39.2	33.2	42.4	30.6	29.0	44.4	40.1	31.7
Nb	0.91	0.92	4.08	0.64	0.82	1.49	0.56	0.91	4.27
La	7.85	8.67	24.3	8.11	14.9	35.0	8.11	8.57	53.1
Ce	31.5	33.1	68.1	33.3	53.0	86.5	31.0	32.9	105.3
Pr	5.29	5.52	9.43	5.36	8.14	10.80	5.00	5.59	11.40
Nd	23.8	24.1	38.0	24.0	33.4	37.5	24.1	27.2	39.3
Sm	3.72	3.87	4.53	4.21	4.63	4.07	3.87	4.12	4.44
Eu	0.93	1.13	1.00	0.93	0.96	0.88	0.98	1.01	0.80
Gd	2.26	2.21	2.46	2.16	2.36	1.87	2.61	2.80	1.94
Tb	0.26	0.24	0.23	0.26	0.20	0.17	0.32	0.27	0.14
Dy	1.36	1.35	1.18	1.50	1.01	0.69	1.49	1.36	0.98
Ho	0.22	0.22	0.14	0.20	0.15	0.09	0.20	0.21	0.10
Er	0.51	0.52	0.42	0.48	0.36	0.21	0.49	0.51	0.28
Tm	0.05	0.05	0.06	0.06	0.03	0.01	0.05	0.07	0.02
Yb	0.30	0.32	0.21	0.35	0.23	0.10	0.27	0.27	0.21
Lu	0.05	0.03	0.03	0.04	0.03	0.01	0.03	0.04	0.02
Hf	1.26	1.40	1.29	1.24	1.20	1.32	1.59	1.37	1.54
Ta	0.11	0.11	0.21	0.10	0.09	0.07	0.10	0.12	0.21
Th	0.06	0.09	0.48	0.07	0.10	1.07	0.06	0.09	1.73
U	0.08	0.05	0.11	0.05	0.02	0.21	0.02	0.04	0.85

In the distribution of Zr/Hf and Ti/Eu (Fig. 5, *b*), all garnets correspond to the field of carbonatite mantle metasomatism [18]. Garnets with a fractionated spectrum from LREE to HREE with minimal concentrations of LREE (0.5-2 ch.u) and without depletion in Eu are close in composition to garnets of Lz-2 type from xenoliths of lherzolites in V.Grib pipe [22] differing from them by higher contents of LREE and MREE (Fig.4, *e*, *f*) and Zr/Hf values (Fig.5, *b*).

Clinopyroxene (Table 3) in sample G2-35 is represented by diopside with a high content of Cr_2O_3 (2.0-3.6 wt.%), i.e., Cr-diopside [23]. Cr-diopside grains in the sample have a heterogeneous composition with varying concentrations of Al_2O_3 (1.9-4.6 wt.%), Cr_2O_3 (2.0-3.6 wt.%), MgO (13.5-15.8 wt.%), CaO (17.3-20.1 wt.%) and Na_2O (2.5-4.6 wt.%); Mg# values 0.93-0.95. All Cr-diopside grains are characterized by a homogeneous composition within the grain. As regards Al_2O_3 and Cr_2O_3 concentrations, all Cr-diopside grains correspond to the field of "cratonic" peridotites [23] and are identical in composition to Cr-diopsides from xenoliths of lherzolites in V.Grib pipe (Fig.6, *a* [22, 24, 25]).

Based on the concentrations of RE and REE, Cr-diopsides (see Table 2) are represented by two types (Fig.6, *c*, *d*). The first type combines grains containing LREE at the level of 30-60 ch.u., with La_n/Yb_n values of 17-85 and Ti/Eu from 650 to 850; the compositions of these grains correspond to the field of silicate metasomatism (see Fig.5, *c*). The second type combines grains with higher LREE concentrations, at the level of 150-225 ch.u., with La_n/Yb_n values from 170 to 240 and Ti/Eu from 1,100 to 1,200; the composition points of these grains do not show a clear correspondence to the fields of either carbonatite or silicate metasomatism (see Fig.5, *c*). According to the concentrations of both main and rare elements, and the nature of the distribution spectra of RE and REE, Cr-diopsides from sample G2-35 are identical to those from xenoliths of lherzolite in V.Grib pipe (Fig.6, *c, d* [22, 24]).

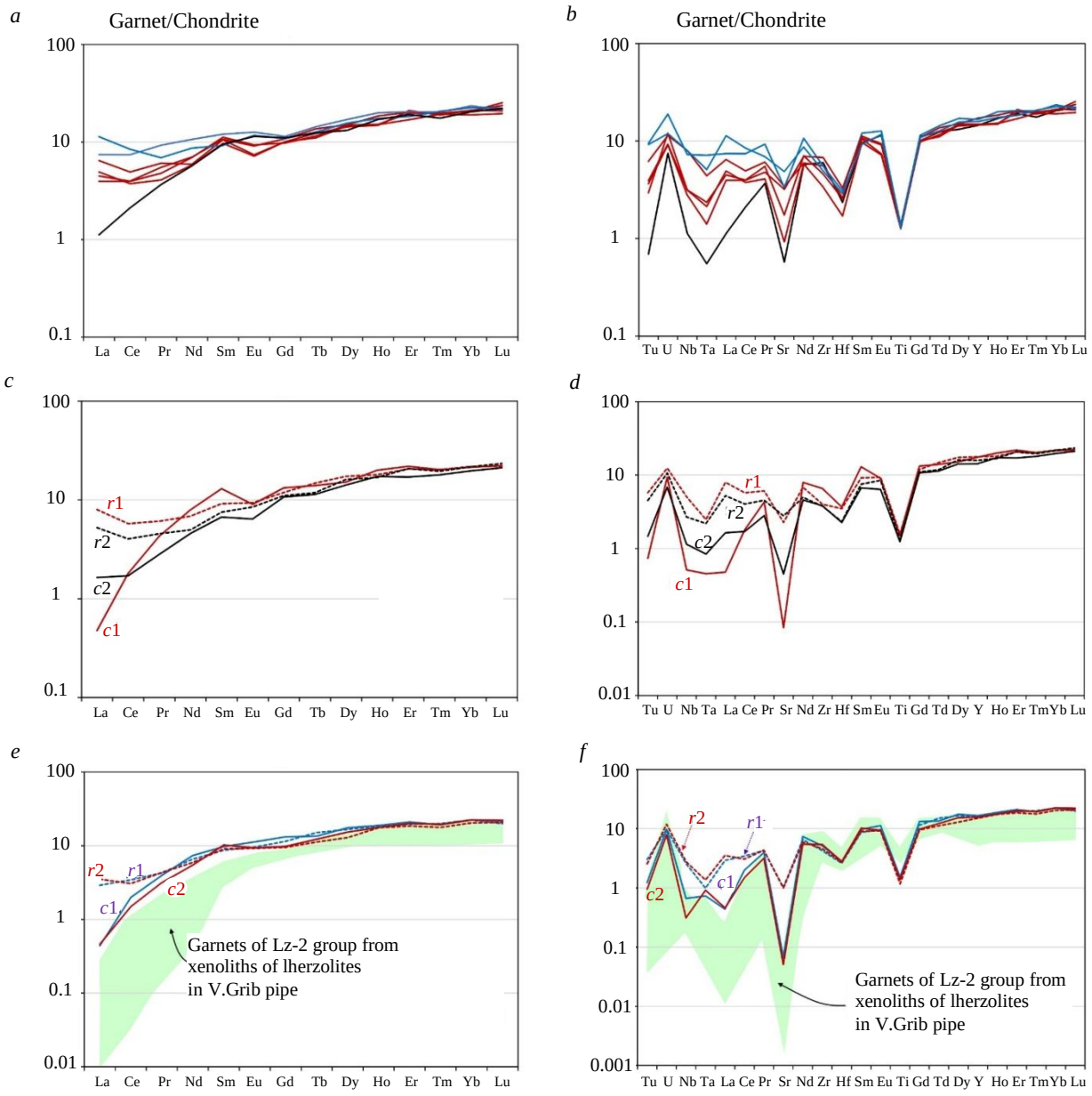

Fig.4. REE (*a*, *c*, *e*) and REE (*b*, *d*, *f*) concentrations normalized to Cl chondrite [20] in garnets from xenolith G2-35:
a, *b* – three types of RE distribution (shown in different colours) in the central parts of grains that are not zoned by RE;
c-*f* – central (*c*1, *c*2) and rim (*r*1, *r*2) parts: *c*, *d* – garnet grains zoned by RE,
e, *f* – garnet grains zoned by REE, similar in composition to Lz-2 garnets from lherzolites in V.Grib pipe [22]

Given a possible coexistence of garnet with olivine, the values of design temperatures (*T*) of the last equilibrium of garnets [26] are in the following ranges: 850-950 °C for most grains, a single value – 1,100, 880 and 980 °C for the central and rim parts, respectively, for Ni-zoned grains. Design values of *P*-*T*-parameters [27] for Cr-diopsides, the compositions of which meet the conditions of [27], vary: T = 760-880 °C and P = 31-35 kbar, which corresponds to the depth interval ~ 95-105 km. The points of design values of *P*-*T*-parameters lie in the region of heat fluxes of lithospheric mantle of 37-40 mV/m^2 (Fig.6, *b* [28]) and correspond to *P*-*T*-parameters of the stability field of graphite [29] and coesite [1].

Discussion of results. It is presumed that at the initial stages of its formation, cratonic lithospheric mantle underwent partial melting with formation of depleted harzburgites and dunites, which subsequently experienced repeated exposure to metasomatic agents of different composition. This led to refertilization of initially depleted mantle rocks [18, 21, 30]. Direct evidence of transition of high-

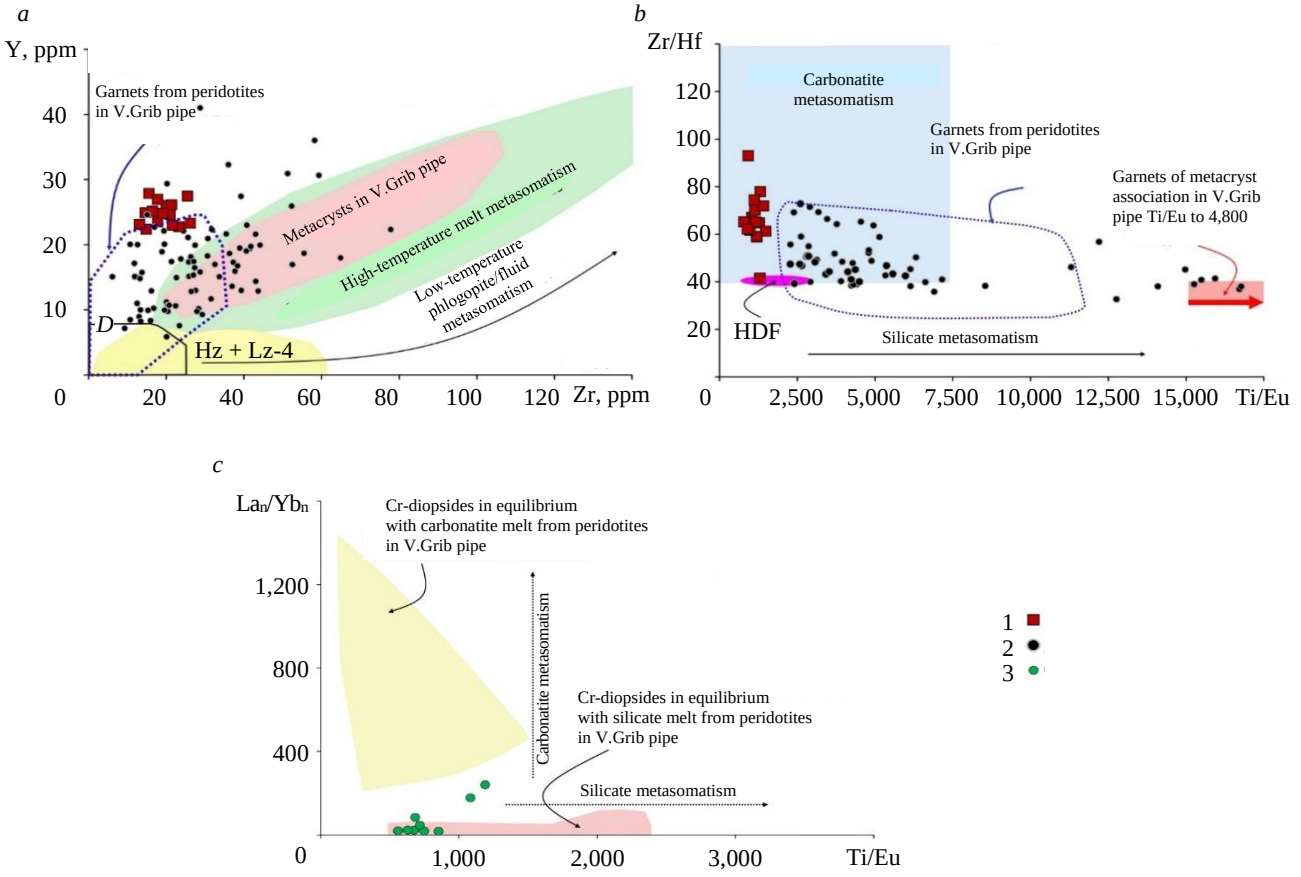

Fig.5. Specific features of compositions of garnet (*a*, *b*) and clinopyroxene (*c*) from xenolith G2-35:
a – position of garnet composition points in comparison with garnets from peridotites in V.Grib pipe [22] on the Y-Zr diagram [21]; *b* – Zr/Hf and Ti/Eu ratios in garnets in comparison with xenocrysts of Lz-2 type garnets in V.Grib pipe [22, 24]; *c* – La_n/Yb_n and Ti/Eu ratios in clinopyroxenes in comparison with Cr-diopsides from peridotites in V.Grib pipe [22]

1 – G2-35 garnets; 2 – xenocrysts of Lz-2 garnets in V.Grib pipe; 3 – Cr-diopsides G2-35
D – field of "depleted" garnets [21]; Hz and Lz-4 – high-chromium garnets of harzburgite and lherzolitic associations with sinusoidal spectra of REE distribution in V.Grib pipe [22]; HDF – high density fluid [18]

chromium harzburgite to lherzolite and subsequent modification of lherzolite are zoned garnets in peridotites of different kimberlites [21, 30]. Concentrations of rare and rare earth elements in rock-forming minerals are important and mandatory components in reconstructing the conditions of formation and alteration of rocks of various genesis [31-33]. The final stage of alteration of garnets of the lherzolite association is recorded by a progressive trend of a simultaneous decrease in the concentrations of Cr_2O_3 and CaO with increasing concentrations of Y and Zr and Ti/Eu values during the silicate mantle metasomatism [18, 21, 30]. Compositions of garnets from sample G2-35 show a progressive trend of simultaneous decrease in the concentrations of Cr_2O_3 and CaO pointing to buffering by clinopyroxene [30]. It can be presumed that the most high-calcium-high-chromium pyropes from sample G2-35 reflect the composition of garnet of the source lherzolite (type Lz-2; see Fig.4, *e*, *f*) which was subsequ ently exposed to high-temperature silicate melt. This led to the enrichment of the rock with modal clinopyroxene [30] and transformation of garnet lherzolite into garnet clinopyroxenite/garnet clinopyroxene rock. Geochemical characteristics of most Cr-diopside grains from sample G2-35 point to the impact of silicate melt. Nevertheless, garnet grains from sample G2-35, which retained a flat (normal) spectrum in the MREE-HREE region, are enriched to varying degrees in LREE and MREE compared to garnets of the Lz-2 type from peridotites in V.Grib pipe, which is indicative of subsequent episodes of their metasomatic enrichment. This is also confirmed by zoning by the main and rare elements within the grains (see Fig.3, *b*), and the values of Zr/Hf and Ti/Eu, which are not characteristic of silicate mantle metasomatism (see Fig.5, *b*).

Journal of Mining Institute. 2024. Vol. 268. P. 503-519

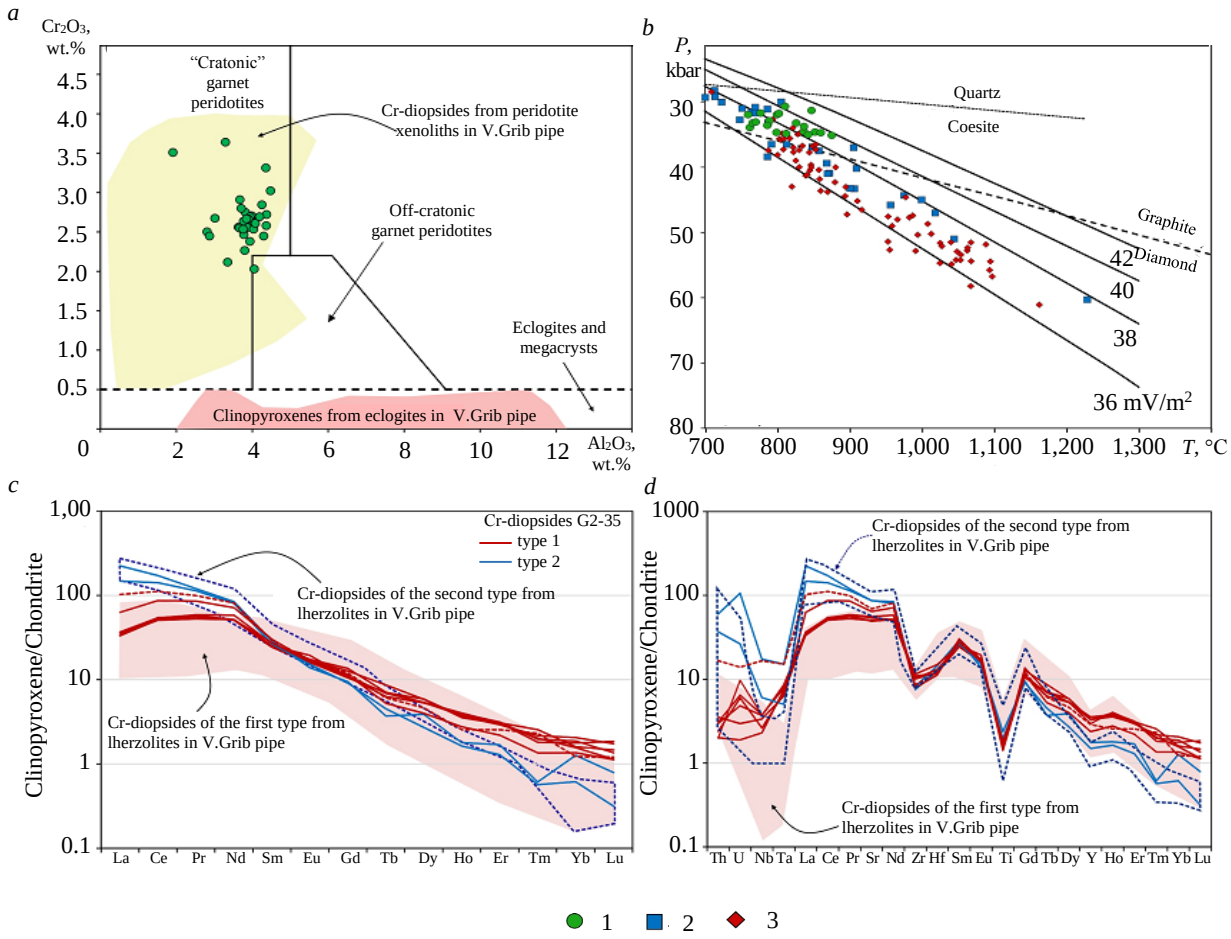

Fig.6. Specific features of composition of Cr-diopside from xenolith G2-35
a – position of composition points for Cr_2O_3 and Al_2O_3 on diagram [23]:
Cr-diopsides from peridotite xenoliths in V.Grib pipe [22, 24, 25]; clinopyroxenes from eclogites in V.Grib pipe [34];
b – position of points of calculated *P-T*-parameters [27] on geotherms of cratonic lithospheric mantle [28];
transition lines graphite – diamond [29], quartz – coesite [1];
c, *d* – normalized to chondrite Cl [20] concentrations of rare earth (*c*) and rare (*d*) elements in two types of Cr-diopside; data on Cr-diopsides from lherzolites in V.Grib pipe [22]
1 – Cr-diopsides G2-35; 2 – lherzolites in V.Grib pipe; 3 – xenocrysts from kimberlite in V.Grib pipe

A distinctive feature of most garnets from sample G2-35 is a negative Eu anomaly (see Fig.4). This anomaly is diagnosed in garnets of mantle eclogites of subduction genesis [7, 8] and is indicative of participation in the petrogenesis of these rocks of a component/melt that had undergone fractionation of plagioclase. Depletion in Eu is typical for garnets from lower crustal granulites and pyroxenites in V.Grib pipe [34]. However, the typical mantle composition of garnet and clinopyroxene from sample G2-35 differs from those from lower crustal rocks and eclogites and pyroxenites of subduction genesis. It was ascertained that high-magnesium eclogites occurring as xenoliths in kimberlites could be a product of intense modification of low-magnesium eclogites of subduction genesis [35] or result from the interaction of silicate melts of subduction genesis with peridotites of the lithospheric mantle [36]. Garnets and clinopyroxenes from such samples contain lower concentrations of Cr_2O_2 (< 1 wt.%), which do not correspond to the mineral composition of sample G2-35, and metasomatic enrichment can lead to the appearance of false positive, but not negative Eu anomalies [35]. Article [24] describes peridotite (N 634) with the rim part of zoned garnet depleted in Cr_2O_3 and CaO and enriched in TiO_2, LREE and MREE relative to the central one, and a weak negative anomaly in Eu is diagnosed in REE distribution. The emplacement of this garnet is associated with the influence of protokimberlite melt enriched in Fe, Ti and REE [24]. This model cannot be applied to garnets from sample G2-35: the central and rim parts of these garnets are depleted in TiO_2 and show no differences in its concentrations;

progressive enrichment of the rim parts of these grains with LREE and MREE is accompanied by a decrease in the Eu anomaly values (see Fig.4). REE concentrations in garnets with a negative Eu anomaly are identical to garnets that retain a flat spectrum in the MREE-HREE region, and the enrichment of the latter in LREE and MREE does not lead to Eu depletion. The appearance of a negative Eu anomaly in garnet sample G2-35 could be associated with the influence of a fluid, the subduction genesis of which cannot be excluded.

Table 3

Concentration of main elements in clinopyroxenes from xenolith G2-35, wt.%

Element	1 *c*	2 *c*	3 *c*	4 *c*	5 *c*	6 *c*	7 *c*	8 *c*
SiO_2	55.45	55.38	55.27	55.49	55.26	55.27	55.40	55.62
TiO_2	0.09	0.10	0.15	0.10	0.09	0.11	0.09	0.11
Al_2O_3	3.80	3.64	2.88	4.05	3.87	3.66	3.76	4.04
Cr_2O_3	2.26	2.56	2.45	2.03	2.56	2.55	2.53	2.54
FeO	1.72	1.74	1.39	1.85	1.76	1.72	1.83	1.82
MnO	0.07	0.08	0.07	0.09	0.05	0.07	0.06	0.07
MgO	14.34	14.55	15.51	14.46	14.18	14.58	14.38	14.02
CaO	18.35	18.18	19.49	17.78	17.84	18.13	17.95	17.82
Na_2O	3.28	3.25	2.48	3.44	3.61	3.38	3.43	3.67
K_2O	0.02	0.01	0.00	0.01	0.00	0.00	0.01	0.00
Total	99.39	99.50	99.67	99.29	99.23	99.48	99.45	99.70
Mg#	0.94	0.94	0.95	0.93	0.93	0.94	0.93	0.93
Element	9 *c*	10 *c*	11 *c*	12 *c*	13 *c*	13 *r*	14 *c*	14 *r*
SiO_2	55.49	55.51	55.65	55.37	54.81	54.95	55.13	55.10
TiO_2	0.10	0.10	0.12	0.11	0.13	0.14	0.12	0.13
Al_2O_3	4.30	3.82	4.08	4.38	4.48	4.25	4.51	4.74
Cr_2O_3	2.45	2.75	2.61	2.72	3.02	2.84	2.81	2.94
FeO	1.72	1.69	1.79	1.75	1.80	1.58	1.82	1.83
MnO	0.06	0.06	0.07	0.08	0.06	0.06	0.09	0.07
MgO	14.26	14.20	14.01	14.16	13.80	14.19	13.90	13.46
CaO	17.70	17.95	17.68	17.50	17.40	17.77	17.57	17.32
Na_2O	3.63	3.53	3.56	3.57	4.47	4.15	4.31	4.59
K_2O	0.00	0.00	0.00	0.00	0.00	0.00	0.02	0.03
Total	99.72	99.59	99.57	99.64	99.98	99.93	100.27	100.20
Mg#	0.94	0.94	0.93	0.94	0.93	0.94	0.93	0.93

The enrichment of LREE, Sr, Th, U, Nb and Ta (see Fig.4), which is recorded in most garnet grains and some grains of Cr-diopsides (see Fig.6, *c*, *d*), points to the influence of LREE-enriched fluid/melt. Low concentrations of Fe and Ti in garnets of sample G2-35 exclude the influence of kimberlite/proto-kimberlite melt [24, 30], and similar contents of Hf, Zr and Ti (see Fig.4, 5, *b*) in garnets – of high-charged elements-enriched fluid of subduction genesis [34]. LREE enrichment of garnets and clinopyroxenes in peridotites can be associated with the influence of carbonatite melt/fluid, which also leads to enrichment of garnets in CaO [18, 21, 30]. Enrichment of garnets of sample G2-35 in LREE is accompanied by a reverse pattern – a decrease in CaO concentration (see Fig.3), which is typical for garnets exposed to the influence of silicate melt [21, 30]. Distribution coefficients (KD) of RE between different types of garnets and Cr-diopsides of sample G2-35 do not correspond to those in equilibrium with carbonatite melt [37]. Composition of the melt which is in equilibrium with LREE-enriched garnets of sample G2-35 (KD [37]) can, in general, be compared with compositions of carbonatites in oceanic environment and the design composition of carbonatite melt [37]

as regards the concentrations of LREE, Sr, Th, U, Nb and Ta, but contains lower concentrations of Zr, Hf, Ti and HREE (Fig.7, *a*). Design composition of the melt in equilibrium with Cr-diopsides (DC [37]) is marked by much higher concentrations of LREE, MREE, Sr, Th, U, Nb and Ta (Fig.7, *b*), which are not comparable with natural and experimental compositions of carbonatites. A fluid enriched in these incompatible elements can be considered as a metasomatic agent, the influence of which led to enrichment of garnets and chromium diopsides in LREE, Sr, Th, U, Nb and Ta. The majority of garnet grains that are not zoned by RE are enriched in LREE, Sr, Th, U, Nbб and Ta, but remain depleted in Eu, which can point to both a successive influence of the fluid of subduction genesis and the fluid enriched in incompatible elements, and their associative character.

In addition to several stages of metasomatic enrichment identified by the compositions of garnets and clinopyroxenes, quartz was found in G2-35. Its formation can be associated with several factors: post-magmatic alteration of kimberlite; regressive transformation of coesite into quartz; carbonatization of mantle rocks; influence of fluid/melt of subduction genesis.

In kimberlite pipes, quartz can be one of numerous secondary minerals forming as a result of post-magmatic processes, or it can be a disintegrated product of the host rocks [38]. In ADP kimberlite pipes, quartz is distributed in crater parts composed of sedimentary and volcanogenic sedimentary rocks containing disintegrated material of enclosing sandstones [16]. Among the processes of secondary mineralization in V.Grib pipe, carbonatization, silicification, saponitization, and ferruginization are common. The development of quartz veinlets was recorded in rocks in the upper part of the pipe to a depth of 200 m and in zones adjacent to the host rocks [39]. Sample G2-35 was taken from kimberlite of the diatreme part of the pipe at the depth of 400 m from the surface, where the minimal presence or complete absence of disintegrated material of enclosing rocks can be initially presumed [39]. Xenolith – kimberlite contact is distinct, xenolith proper is framed by a thin chlorite rim. Large-scale or vein development of secondary mineralization is not recorded either at the rock contact or in kimberlite proper. In xenolith, quartz does not develop along cracks in minerals or intergranular space and does not have the forms of veins or druses characteristic of secondary quartz in kimberlite pipes [38]. Postmagmatic minerals typical of association with secondary quartz (for example, calcite, pyrite, magnetite, goethite, etc.) were not found either as inclusions in quartz or in xenolith proper. Quartz grains in sample G2-35 are oval or elongated and have distinct boundaries with garnet and clinopyroxene. The above data indicate that quartz in sample G2-35 is not a secondary mineral forming as a result of post-magmatic processes.

In samples of cratonic lithospheric mantle, the appearance of quartz is associated with transformation of coesite as a result of pressure decrease [6, 8, 10]. The study of natural samples and experimental studies [5, 6, 40] showed that coesite replacement with quartz is accompanied by appearance of specific structural and morphological features: intense fracturing or appearance of radial cracks

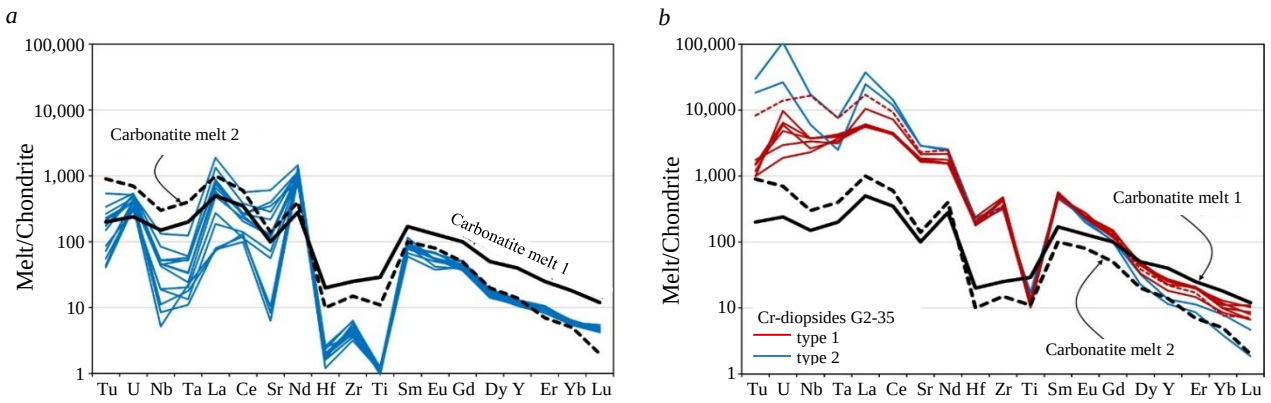

Fig.7. Concentrations of rare elements normalized to Cl chondrite [20] in design melt compositions in equilibrium with garnets (*a*) and two types of Cr-diopsides (*b*) from xenolith G2-35. Compositions of carbonatite melts and KD [37]

around the grain; elongated shape of quartz crystals with development of their long axes perpendicular to the boundary of the replaced grain; well-formed "palisade" structures; mosaic structure with angular, "jagged" boundaries of quartz grains; polygonal structure of quartz. The above described structural and morphological features are not recorded in quartz grains of sample G2-35. Relics of coesite were not found in sample G2-35. However, the calculated *P-T*-parameters of Cr-diopsides from sample G2-35 indicate its capture from the depth interval ~ 95-105 km (31-35 kbar), and *T* values vary from 760 to 880 °C, which corresponds to the stability field of coesite and does not allow excluding that quartz in sample G2-35 can represent paramorphs after coesite.

Detection of SiO_2 in the form of coesite or quartz (as a paramorph after coesite) in samples of mantle eclogites is direct evidence of non-mantle origin of their protoliths [7, 8, 41]. Coesite or quartz (as a paramorph after coesite) are diagnosed as inclusions in diamond crystals of eclogite (E-type), less frequently websterite (W-type) types [18]. The existence within a diamond crystal of mineral parageneses of mixed peridotite-eclogite type [9, 10] can indicate both the participation of deeply subducted crustal material in the process of diamond growth [9] and a staged nature of diamond growth as a result of a marked change in the composition of the crystallization medium [10] associated with successive carbonatization reactions of peridotites, the final result of which is the formation of magnesite and free SiO_2 [10, 11]. As a result of carbonatization of eclogites, free SiO_2 can also form followed by crystallization of quartz or coesite, accompanied by formation of magnesite [42] or dolomite [43], as shown in experimental works [42, 43]. Taking into account the results of experimental studies and the actual mineral association of sample G2-35, a model for the formation of SiO_2 phase (quartz/coesite) as a result of carbonatization of mantle rocks can be considered. It can be presumed that at the time of quartz formation the rock was garnet clinopyroxenite/garnet-clinopyroxene and not olivine ± orthopyroxene-bearing lherzolite.

Fluid infiltration into the continental lithospheric mantle is an important factor controlling sudden changes in its chemical and physical properties and represents the medium for the generation and growth of diamonds [44]. Compositions of such fluids – high-density fluids or HDF – are known from the study of fluid inclusions in diamond crystals with a fibrous structure [44, 45] and are represented by four types: silicic, low-magnesium carbonatite, high-magnesium carbonatite, and saline. High concentrations of volatile components and strong enrichment in incompatible elements of all types of HDF allow considering them as efficient metasomatic agents. It was ascertained [44] that the formation of high-magnesium HDF is associated with melting of carbonate-containing peridotite, while silicic and low-magnesium carbonatite HDF are the result of low degrees of partial melting of carbonate-containing eclogite. The genetic association of silicic HDF and eclogites is confirmed by numerous occurrences of fluid inclusions of such composition in association with E-type inclusions in diamond crystals with a fibrous structure, including quartz [46]. Paper [44] shows a possibility of direct influx of saline HDF into rocks of lithospheric mantle in the process of subduction, which causes *in situ* melting of carbonate-containing peridotites and eclogites with subsequent formation of high-magnesium HDF and silicic and low-magnesium carbonatite HDF, respectively. High-magnesium carbonatite and silicic HDF were discovered in cuboid type diamonds in V.Grib pipe [45]. Thus, the model for the formation of SiO_2 phase (quartz/coesite) in G2-35 xenolith as a result of exposure to silicic HDF genetically related to eclogites, can be considered. Signs of the influence of subduction-related fluid were recorded in samples of zircon-bearing eclogites in V.Grib pipe, the formation of which belongs to the Paleoproterozoic (1.9-1.7 Ga) subduction stage. According to article [34], these eclogites were captured from the depth of ~120 km, which is close to the design parameters of Cr-diopsides from sample G2-35 (~95-105 km).

Formation of quartz as a result of interaction of SiO_2-enriched melt of subduction genesis with peridotites of lithospheric mantle was proposed for several unique xenoliths of lithospheric mantle discovered in alkali basalts of volcanic fields Bakoni-Balaton-Highland in western Hungary [3] and

Tallante province in southern Spain [4]. In these samples, quartz occurs as inclusions in ortho- and clinopyroxenes and olivine-free websterite enriched in orthopyroxene [3] and in orthopyroxene of peridotites [4]. SiO_2-enriched melt inclusions in orthopyroxene were also discovered, and a peridotite sample [4] bordering on a felsic vein formation composed of orthopyroxene, plagioclase and quartz through an orthopyroxene-rich reaction zone. SiO_2 enrichment of peridotites in cratonic lithospheric mantle is revealed by higher Si/Mg values and an increased content of modal orthopyroxene coexisting with high-magnesium olivine [46]. One of several different models that explain the increase in SiO_2 concentrations in depleted peridotites [46] is reaction with melt formed during melting of residual or subduction eclogites [47], which results in formation of orthopyroxene-enriched peridotites or pyroxenites that do not contain olivine [48], with increasing melt/peridotite ratio, respectively. Enrichment in modal orthopyroxene (to 18-30 vol.%) is recorded in several samples of garnet peridotites in V.Grib pipe [22]. In sample G2-35, orthopyroxene was not found, which allows only assuming a possible transition of olivine-containing lherzolite into orthopyroxene-enriched pyroxenite under the influence of SiO_2 melt with subsequent formation of quartz without preservation of orthopyroxene. Formation of Cr-pyrope of the lherzolite association as a product of exsolution of orthopyroxene, including in association with Cr-diopside, is described in a series of articles [49]. Concentrations of the main elements in pyrope and Cr-diopside from sample G2-35 are comparable to those from article [49]. There are known occurrences of SiO_2 phase (quartz/coesite) as an exsolution product of garnet or clinopyroxene in samples of UHP-metamorphic rocks [50], but in samples of cratonic lithospheric mantle they occur as exsolution structures only in garnets of eclogites of subduction genesis [6]. Coexistence of SiO_2 phase in association with high-chromium mantle minerals as exsolution structures was not described earlier. At reaction of SiO_2-rich melts that form during partial melting of eclogites under subduction with peridotites of lithospheric mantle, garnet-clinopyroxene rocks that do not contain olivine can form [48]. However, compositions of garnets and clinopyroxenes forming in this reaction correspond to those of group A eclogites or websterites [36] which have an intermediate composition between low-magnesium group B eclogites and peridotites and contain much lower concentrations of Cr_2O_3 (<0.5 wt.% [48]), not comparable with compositions of pyropes and Cr-diopsides from sample G2-35.

Conclusion. The first data on the composition of rock-forming minerals of the unique mantle xenolith in V.Grib kimberlite pipe, which presents a previously undescribed mineral association of Cr-pyrope, Cr-diopside and quartz were obtained. The interpretation of data on concentrations of the main and rare elements in Cr-pyrope and Cr-diopside allowed reconstructing the stages of rock transformation as a result of the influence of metasomatic agents. The influence of high-temperature silicate melts led to transformation of the source lherzolite into a rock enriched in clinopyroxene and garnet, which was identified from the progressive trend of a simultaneous decrease in Cr_2O_3 and CaO concentrations in pyropes and preservation of "normal" REE distribution spectra identical to those in pyropes of lherzolites in V.Grib pipe. Subsequent stages of exposure to metasomatic agents are recorded from the occurrence of a pronounced negative Eu anomaly in pyropes, which can be caused by the influence of subduction-related fluid, and enrichment of LREE, Sr, Th, U, Nb and Ta pyropes and Cr-diopsides as a result of the presence of fluid enriched in these incompatible elements.

It was shown that quartz in the studied xenolith was not a secondary mineral forming as a result of the influence of post-magmatic processes. The absence of specific structural and morphological features accompanying coesite replacement by quartz does not allow to unambiguously state that SiO_2 initially present in the sample was coesite. However, the calculated *P-T*-parameters of Cr-diopsides from sample G2-35 indicate its capture from the depth interval of ~ 95-105 km (31-35 kbar) corresponding to coesite stability field, which does not exclude the possibility that quartz in xenolith can be paramorphs after coesite.

As priority models for the formation of SiO_2 phase (quartz/coesite) in mantle xenolith G2-35, we consider carbonatization of mantle peridotites or eclogites and the influence of silicic fluid (HDF) formed during melting of carbonate-containing eclogites at subduction stage. These models can also explain the enrichment of garnets and clinopyroxenes with LREE, Sr, Th, U, Nb and Ta. The absence of reaction zones, orthopyroxene relics, melt inclusions and exsolution structures in minerals in sample G2-35 as well as high concentrations of Cr_2O_3 in garnet and clinopyroxene do not allow considering the model of SiO_2 phase formation as a result of interaction of SiO_2-enriched melt of subduction genesis with peridotites of lithospheric mantle as a priority at this stage of the study. The enrichment of lithospheric mantle rocks in SiO_2 with subsequent formation of SiO_2 phase (quartz/coesite) in association with high-chromium mantle minerals, apparently, had a local character.

Results of the study showed a possibility of coexistence of SiO_2 phase (quartz/coesite) in association with high-chromium mantle minerals within the natural xenolith of cratonic lithospheric mantle. The data obtained can be used to interpret the results of both experimental studies and the study of natural samples of lithospheric mantle, which contain mineral associations of "mixed" peridotite pyroxenite-eclogite types.

REFERENCES

1. Bose K., Ganguly J. Quartz-coesite transition revisited: Reversed experimental determination at 500-1200 °C and retrieved thermochemical properties. *American Mineralogist*. 1995. Vol. 80, p. 231-238. DOI: 10.2138/am-1995-3-404

2. Incel S., Milke R., Wunder B. Orthopyroxene rim growth during reaction of (Co, Ni, Mn, Zn)-doped forsterite and quartz: Experimental constraints on element distribution and grain boundary diffusion. *Mineralogy and Petrology*. 2022. Vol. 116, p. 137-149. DOI: 10.1007/s00710-022-00773-3

3. Bali E., Zajacz Z., Kovacz I. et al. A Quartz-bearing Orthopyroxene-rich Websterite Xenolith from the Pannonian Basin, Western Hungary: Evidence for Release of Quartz-saturated Melts from a Subducted Slab. *Journal of Petrology*. 2008. Vol. 49. N 3, p. 421-439. DOI: 10.1093/petrology/egm086

4. Dallai L., Bianchini G., Avanzinelli R. et al. Quartz-bearing rhyolitic melts in the Earth's mantle. *Nature Communications*. 2022. Vol. 13. N 7765, p. 1-9. DOI: 10.1038/s41467-022-35382-3

5. Mikhailenko D.S., Aulbach S., Korsakov A. et al. Origin of Graphite-Diamond-Bearing Eclogites from Udachnaya Kimberlite Pipe. *Journal of Petrology*. 2021. Vol. 62. N 8, p. 1-32. DOI: 10.1093/petrology/egab033

6. Alifirova T.A., Pokhilenko L.N., Korsakov A.V. Apatite, SiO_2, rutile and orthopyroxene precipitates in minerals of eclogite xenoliths from Yakutian kimberlites, Russia. *Lithos*. 2015. Vol. 226, p. 31-49. DOI: 10.1016/j.lithos.2015.01.020

7. Aulbach S., Smart K.A. Petrogenesis and Geodynamic Significance of Xenolitic Eclogites. *Annual Review of Earth and Planetary Sciences*. 2023. Vol. 51, p. 521-549. DOI: 10.1146/annurev-earth-031621-112904

8. Mikhailenko D., Golovin A., Korsakov A. et al. Metasomatic Evolution of Coesite-Bearing Diamondiferous Eclogite from the Udachnaya Kimberlite. *Minerals*. 2020. Vol. 10. N 383. DOI: 10.3390/min10040383

9. Zuowei Yin, Cui Jiang, Meihua Chen et al. Inclusions of α-quartz, albite and olivine in a mantle diamond. *Gondwana Research*. 2017. Vol. 44, p. 228-235. DOI: 10.1016/j.gr.2016.12.004

10. Stachel T., Harris J.W., Brey G.P. Rare and unusual mineral inclusions in diamonds from Mwadui, Tanzania. *Contributions to Mineralogy and Petrology*. 1998. Vol. 132, p. 34-47. DOI: 10.1007/s004100050403

11. Shatskiy A., Litasov K.D., Sharygin I.S., Ohtani E. Composition of primary kimberlite melt in a garnet lherzolite mantle source: constraints from melting phase relations in anhydrous Udachnaya-East kimberlite with variable CO_2 content at 6.5 GPa. *Gondwana Research*. 2017. Vol. 45, p. 208-227. DOI: 10.1016/j.gr.2017.02.009

12. Stativko V.S., Skublov S.G., Smolenskiy V.V., Kuznetsov A.B. Trace and rare-earth elements in garnets from silicate-carbonate formations of the Kusa-Kopan complex (Southern Urals). *Lithosphere (Russia)*. 2023. Vol. 23. N 2, p. 225-246 (in Russian). DOI: 10.24930/1681-9004-2023-23-2-225-246

13. Skublov S.G., Gavrilchik A.K., Berezin A.V. Geochemistry of beryl varieties: comparative analysis and visualization of analytical data by principal component analysis (PCA) and t-distributed stochastic neighbor embedding (t-SNE). *Journal of Mining Institute*. 2022. Vol. 255, p. 455-469. DOI: 10.31897/PMI.2022.40

14. Skublov S.G., Rumyantseva N.A., Qiuli Li et al. Zircon Xenocrysts from the Shaka Ridge Record Ancient Continental Crust: New U-Pb Geochronological and Oxygen Isotopic Data. *Journal of Earth Science*. 2022. Vol. 33. N 1, p. 5-16. DOI: 10.1007/s12583-021-1422-2

15. Larionova Yu.O., Sazonova L.V., Lebedeva N.M. et al. Kimberlite Age in the Arkhangelsk Province, Russia: Isotopic Geochronologic Rb-Sr and $^{40}Ar/^{39}Ar$ and Mineralogical Data on Phlogopite. *Petrology*. 2016. Vol. 24. N 6, p. 607-639. DOI: 10.7868/S0869590316040026

16. Ustinov V.N., Mikoev I.I., Piven G.F. Prospecting models of primary diamond deposits of the north of the East European Platform. *Journal of Mining Institute*. 2022. Vol. 255, p. 299-318. DOI: 10.31897/PMI.2022.49

17. Kargin A.V., Nosova A.A., Sazonova L.V. et al. Ultramafic Alkaline Rocks of Kepino Cluster, Arkhangelsk, Russia: Different Evolution of Kimberlite Melts in Sills and Pipes. *Minerals*. 2021. Vol. 11. N 540. DOI: 10.3390/min11050540

18. Stachel T., Aulbach S., Harris J.W. Mineral Inclusions in Lithospheric Diamonds. *Reviews in Mineralogy and Geochemistry.* 2022. Vol. 88. N 1, p. 307-391. DOI: 10.2138/rmg.2022.88.06

19. Sobolev N.V., Lavrentev Yu.G., Pokhilenko N.P., Usova L.V. Chrome-Rich Garnets from the Kimberlites of Yakutia and Their Parageneses. *Contributions to Mineralogy and Petrology*. 1973. Vol. 40, p. 39-52. DOI: 10.1007/BF00371762

20. McDonough W.F., Sun S.S. The composition of the Earth. *Chemical Geology*. 1995. Vol. 120, p. 223-253. DOI: 10.1016/0009-2541(94)00140-4

21. Griffin W.L., Shee S.R., Ryan C.G. et al. Harzburgite to lherzolite and back again: metasomatic processes in ultramafic xenoliths from the Wesselton kimberlite, Kimberly, South Africa. *Contributions to Mineralogy and Petrology*. 1999. Vol. 134, p. 232-250. DOI: 10.1007/s004100050481

22. Shchukina E.V., Agashev A.M., Kostrovitsky S.I., Pokhilenko N.P. Metasomatic processes in the lithospheric mantle beneath the V.Grib kimberlite pipe (Arkhangelsk diamondiferous province, Russia). *Russian Geology and Geophysics*. 2015. Vol. 56. N 12, p. 2153-2172 (in Russian). DOI: 10.15372/GiG20151204

23. Ramsey R.R., Tompkins L.A. The geology, heavy mineral concentrate mineralogy, and diamond prospectivity of the Boa Esperanca and Cana Verde pipes, Corrego D'anta, Minas Gerais, Brazil. Kimberlites, Related Rocks and Mantle Xenoliths. Fifth International Kimberlite Conference, 18 June – 4 July 1991, Araxá, Brazil. Special Publication: Companhia de Pesquisa de Recursos Minerais, 1994, p. 329-345.

24. Kargin A.V., Sazonova L.V., Nosova A.A., Tretyachenko V.V. Composition of garnet and clinopyroxene in peridotite xenoliths from the Grib kimberlite pipe, Arkhangelsk diamond province, Russia: Evidence for mantle metasomatism associated with kimberlite melts. *Lithos*. 2016. Vol. 262, p. 442-455. DOI: 10.1016/j.lithos.2016.07.015

25. Lebedeva N.M., Nosova A.A., Kargin A.V. et al. Sr-Nd-O isotopic evidence of variable sources of mantle metasomatism in the subcratonic lithospheric mantle beneath the Grib kimberlite, northwestern Russia. *Lithos*. 2020. Vol. 376-377. N 105779. DOI: 10.1016/j.lithos.2020.105779

26. Canil D. The Ni-in-garnet geothermometer: calibration at natural abundances. *Contributions to Mineralogy and Petrology*. 1999. Vol. 136, p. 240-246. DOI: 10.1007/s004100050535

27. Nimis P., Taylor W.R. Single clinopyroxene thermobarometry for garnet peridotites. Part I. Calibration and testing of a Cr-in-Cpx barometer and an enstatite-in-Cpx thermometer. *Contributions to Mineralogy and Petrology*. 2000. Vol. 139, p. 541-554. DOI: 10.1007/s004100000156

28. Hasterok D., Chapman D.S. Heat production and geotherms for the continental lithosphere. *Earth and Planetary Science Letters*. 2011. Vol. 307, p. 59-70. DOI: 10.1016/j.epsl.2011.04.034

29. Day H.W. A revised diamond-graphite transition curve. *American Mineralogist*. 2012. Vol. 97, p. 52-62. DOI: 10.2138/am.2011.3763

30. Agashev A.M., Ionov D.A., Pokhilenko N.P. et al. Metasomatism in lithospheric mantle roots: Constraints from whole-rock and mineral chemical composition of deformed peridotite xenoliths from kimberlite pipe Udachnaya. *Lithos*. 2013. Vol. 160-161, p. 201-215. DOI: 10.1016/j.lithos.2012.11.014

31. Gavrilchik A.K., Skublov S.G., Kotova E.L. Trace Element Composition of Beryl from the Sherlovaya Gora Deposit, South-Eastern Transbaikalia, Russia. *Zapiski RMO (Proceedings of the Russian Mineralogical Society).* 2021. Vol. 150. N 2, p. 69-82 (in Russian). DOI: 10.31857/S0869605521020052

32. Rumyantseva N.A., Skublov S.G., Vanshtein B.G. et al. Zircon from gabbroids of the Shaka Ridge (South Atlantic): U-Pb age, oxygen isotope ratio and rare element composition. *Zapiski RMO (Proceedings of the Russian Mineralogical Society)*. 2022. Vol. 151. N 1, p. 44-73 (in Russian). DOI: 10.31857/S0869605522010099

33. Skuzovatov S., Shatsky V.S., Ragozin A.L., Smelov A.P. The evolution of refertilized lithospheric mantle beneath the northeastern Siberian craton: Links between mantle metasomatism, thermal state and diamond potential. *Geoscience Frontiers.* 2022. Vol. 13. Iss. 6. N 101455. DOI: 10.1016/j.gsf.2022.101455

34. Shchukina E.V., Agashev A.M., Zedgenizov D.A. Origin of zircon-bearing mantle eclogites entrained in the V.Grib kimberlite (Arkhangelsk region, NW Russia): Evidence from mineral geochemistry and the U-Pb and Lu-Hf isotope compositions of zircon. *Mineralogy and Petrology*. 2018. Vol. 112. N 1, p. 85-100. DOI: 10.1007/s00710-018-0581-z

35. Gréau Y., Huang J.-X., Griffin W.L. et al. Type I eclogites from Roberts Victor kimberlites: Products of extensive mantle metasomatism. *Geochimica et Cosmochimica Acta*. 2011. Vol. 75, p. 6927-6954. DOI: 10.1016/j.gca.2011.08.035

36. Taylor L.A., Snyder G.A., Keller R. et al. Petrogenesis of group A eclogites and websterites: evidence from the Obnazhennaya kimberlite, Yakutia. *Contributions to Mineralogy and Petrology*. 2003. Vol. 145. Iss. 4, p. 424-443. DOI: 10.1007/s00410-003-0465-y

37. Dasgupta R., Hirschmann M.M., McDonough W.F. et al. Trace element partitioning between garnet lherzolite and carbonatite at 6.6 and 8.6 GPa with applications to the geochemistry of the mantle and of mantle-derived melts. *Chemical Geology*. 2009. Vol. 262, p. 57-77. DOI: 10.1016/j.chemgeo.2009.02.004

38. Zinchuk N.N. Specific features of postmagmatic and hypergene kimberlite rock alteration research. *Otechestvennaya Geologiya (National Geology)*. 2021. N 5, p. 26-42 (in Russian).

39. Pendelyak R.N., Morozov A.V., Mogutova V.A. Geological structure of the tube V.Griba and its display features in geophysical fields. *Otechestvennaya Geologiya (National Geology).* 2019. N 5, p. 53-59 (in Russian). DOI: 10.24411/0869-7175-2019-10038

40. Bidgood A.K., Parsons A.J., Lloyd G.E. et al. EBSD-based criteria for coesite-quartz transformation. *Journal of Metamorphic Geology*. 2021. Vol. 39. Iss. 2, p. 165-180. DOI: 10.1111/jmg.12566

41. Aulbach S., Arndt N.T. Eclogites as palaeodynamic archives: Evidence for warm (not hot) and depleted (but heterogeneous) Archaean ambient mantle. *Earth and Planetary Science Letters*. 2019. Vol. 505, p. 162-172. DOI: 10.1016/j.epsl.2018.10.025

42. Vinogradova Y.G., Shatskiy A., Arefiev A.V., Litasov K.D. The equilibrium boundary of the reaction $Mg_3Al_2Si_3O_{12} + 3CO_2 = Al_2SiO_5 + 2SiO_2 + 3MgCO_3$ at 3-6 GPa. *American Mineralogist*. 2023, p. 1-24 (Online first). DOI: 10.2138/am-2022-8696

43. Shatskiy A., Vinogradova Y.G., Arefiev A.V., Litasov K.D. Revision of the $CaMgSi_2O_6$–CO_2 *P-T* phase diagram at 3-6 GPa. *American Mineralogist*. 2023, p. 1-21 (Online first). DOI: 10.2138/am-2022-8588

44. Weiss Y., Czas J., Navon O. Fluid Inclusions in Fibrous Diamonds. *Reviews in Mineralogy and Geochemistry.* 2022. Vol. 88. Iss. 1, p. 475-532. DOI: 10.2138/rmg.2022.88.09

45. Zedgenizov D.A., Malkovets V.G., Griffin W.L. Composition of diamond-forming media in cuboid diamonds from the V.Grib kimberlite pipe (Arkhangelsk province, Russia). *Geochemical Journal*. 2017. Vol. 51. Iss. 3, p. 205-213. DOI: 10.2343/geochemj.2.0455

46. Tomlinson E.L., Kamber B.S. Depth-dependent peridotite-melt interaction and the origin of variable silica in the cratonic mantle. *Nature Communications*. 2021. Vol. 12. N 1082. DOI: 10.1038/s41467-021-21343-9

47. Yaxley G.M., Green D.H. Reactions between eclogite and peridotite: mantle refertilisation by subduction of oceanic crust. *Swiss Journal of Geosciences Supplement*. 1998. Vol. 78. Iss. 2, p. 243-255.

48. Rapp R.P., Norman M.D., Laporte D. et al. Continent Formation in the Archean and Chemical Evolution of the Cratonic Lithosphere: Melt-Rock Reaction Experiments at 3-4 GPa and Petrogenesis of Archean Mg-Diorites (Sanukitoids). *Journal of Petrology*. 2010. Vol. 51. N 6, p. 1237-1266. DOI: 10.1093/petrology/egq017

49. *Gibson S.A.* On the nature and origin of garnet in highly-refractory Archean lithospheric mantle: constraints from garnet exsolved in Kaapvaal craton orthopyroxenes. *Mineralogical Magazine*. 2017. Vol. 81. Iss. 4, p. 781-809. DOI: 10.1180/minmag.2016.080.158

50. Keller D.S., Ague J.J. Quartz, mica, and amphibole exsolution from majoritic garnet reveals ultra-deep sediment subduction, Appalachian orogeny. *Science Advances*. 2020. Vol. 6. Iss. 11. DOI: 10.1126/sciadv.aay5178

Authors: **Elena V. Agasheva,** *Candidate of Geological and Mineralogical Sciences, Senior Researcher, helenashchukina@gmail.com, https://orcid.org/0000-0002-9396-8568 (V.S.Sobolev Institute of Geology and Mineralogy, Novosibirsk, Russia*), **Denis S. Mikhailenko,** *Candidate of Geological and Mineralogical Sciences, Senior Researcher, https://orcid.org/0000-0003-0585-3021 (V.S.Sobolev Institute of Geology and Mineralogy, Novosibirsk, Russia),* **Andrei V. Korsakov,** *Doctor of Geological and Mineralogical Sciences, Chief Researcher, https://orcid.org/0000-0002-4922-7658 (V.S.Sobolev Institute of Geology and Mineralogy, Novosibirsk, Russia).*

The authors declare no conflict of interests.